Segmentation and Removal of Interphase Cells from Chromosome Images using Multidirectional Block Ranking

Sivaramakrishnan Rajaraman[1], Ganesh Vaidyanathan[2] and Arun Chokkalingam[3]

[1]*Department of Biomedical Engineering, Sri Sivasubramaniya Nadar College of Engineering, Kalavakkam-603110 - India*
[2]*Department of Electronics and Communication Engineering, Sri Venkateshwara College of Engineering, Sriperampudur-602105 - India*
[3]*Department of Electronics and Communication Engineering, R.M.K. College of Engineering and Technology, Kavarapettai-601206 - India*

sivaramakrishnanr@ssn.edu.in, gvaidyas@svce.ac.in, carunece@gmail.com

Abstract

This paper proposes Multidirectional Block Ranking based segmentation and removal of Interphase cells from chromosome images. The efficiency of automatic karyotyping decreases with the presence of undivided, condensed mass of chromosomes called Interphase cells, stain, debris and other unwanted interferences in the chromosome image. The algorithm segments and removes these interferences and enhances the accuracy of automatic karyotyping. The method is tested and excellent segmentation accuracy is accomplished. The chromosome image is preprocessed and a boundary-mapping algorithm is applied to identify the Region of Interest (RoI). The image is divided into blocks and ranks are assigned to all the blocks using Gaussian Ranking Functions (GRF) based on their contribution to the RoI. A higher rank is assigned to the block contributing more while a lesser rank is assigned to other blocks that contribute less to the RoI. The Interphase cells that constitute the RoI are removed from the chromosome images based on the cumulative rank obtained by the blocks in the chromosome image. The proposed algorithm is applied to segment and remove Interphase cells, stains, dirt and other particles that exhibit structural homogeneity. The algorithm gives accurate results in applications where the RoI to be segmented share the grey level with the background wherein the traditional image segmentation methods fall short of accomplishing precise segmentation results.

Keywords: *Interphase cells, Automatic karyotyping, Multidirectional block ranking, Gaussian Ranking Function (GRF), Cumulative rank, Structural homogeneity, Region of Interest (RoI), Segmentation accuracy*

1. Introduction

Human body contains 24 different classes of chromosomes that are classified in to 22 pairs of autosomes and a pair of sex chromosomes X and Y. Every human body cell carries 46 chromosomes in total that includes 22 pair of autosomes and a pair of sex chromosomes except for the sperm and ovum cells that carry only 23 chromosomes [1]. Figure 1a shows a typical photomicrograph showing the presence of chromosomes along with the Interphase cells. Karyotyping is the process of examining these chromosomes in cells that helps diagnosing the genetic disorders [2, 3]. The karyotype image contains all the chromosomes in a cell, arranged graphically in accordance to the International System for Cytogenetic Nomenclature (ISCN) [4]. Karyotyping is an excellent tool to detect deviations from normal

cell structure since abnormal cells may have an excess or a deficit of chromosomes [5]. The presence of overlapping chromosomes and other unwanted interferences prevented chromosomal examination from being an entirely automatic process. [6, 7]. Irrespective of these limiting factors, the karyotyping process efficiently helps in counting the chromosome numbers in individual cells and visualizes structural alterations in the chromosomes. An enormous amount of research is happening in examining the chromosomes to diagnose genetic disorders [8]. Pixel-wise classification methodologies had also been employed in identifying genetic abnormalities [9]. Figure 1b shows a typical human karyotype.

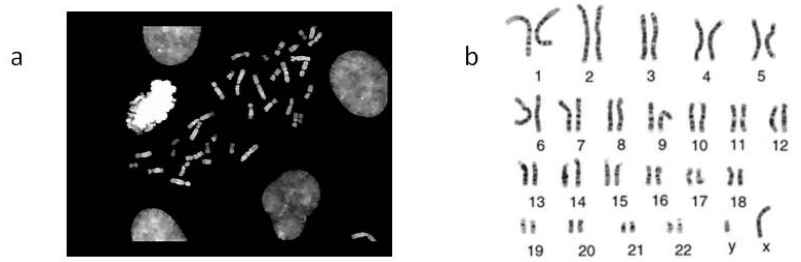

Figure 1. a) Photomicrograph Showing the Presence of Interphase Cells; b) Karyotype

A major difficulty in the segmentation of Interphase cells is that they share their grey levels with the background and the chromosomes [10, 11]. The presence of these limiting factors in a photomicrograph poses serious threat for accurate classification of chromosomes. Thresholding based image segmentation techniques had been proposed [12] but any effort made to remove these Interphase cells based on thresholding and other intensity-based methods, removed the chromosomes with similar intensity levels. Conventional thresholding techniques failed to segment and remove Interphase cells. Nevertheless, the Interphase cells exhibit structural homogeneity that this property can be employed to segment and remove them from the chromosome images. Different statistical parameters such as mean, variance, and entropy are evaluated in multiple directions to ascertain the contribution of blocks to the object of interest and ranks are assigned using Gaussian Ranking Functions (GRF). A block gets higher rank if its contribution is more to an object of interest and lower rank if it is less. By applying Thresholding algorithm on the rank obtained by the blocks, the object of interest can be isolated from the rest of the image. This technique is particularly useful when the background shares the grey levels of the object to be segmented and other objects that are not of interest, wherein the conventional threshold based techniques fail to perform accurate segmentation. The performance of the proposed algorithm is compared with other popular techniques used for segmentation.

2. Materials and Methods

2.1. Boundary mapping using Morphological Operators

A Boundary Mapping algorithm is proposed herewith that detects individual objects in the given image and returns the segmented objects. The Boundary Mapping algorithm makes use of edge detection to compute the threshold value that is further tuned and applied to another edge operator to give a binary mask, containing the objects to be segmented. Applying an edge operation takes the intensity image or a binary image as its input and returns a binary image of exactly the same size, with a value of '1' along the edges and '0' elsewhere. There

are diverse methods of edge detection using different approximations that includes Sobel, Prewitt, Roberts, Laplacian of Gaussian, Zero-cross and Canny but the Sobel approximation gives best results for the problem of interest. The sensitivity threshold and directionality parameters are specified for the Sobel approximation that facilitates accurate determination of edges. A quantity called Fudge Factor is also included to compensate for uncertainty [13]. The Fudge factor is added to the calculation to add an error margin in unknown quantities.

A Morphological structuring element is created within a specified neighborhood, where the 1's location defines the neighborhood for the morphological operation [14]. There are diverse kinds of structuring elements that can be used and a flat linear structuring element that is symmetric with respect to the neighborhood center is used. An angle of 90 degrees and length of '3' is assumed where the degree specifies the angle of the line as measured in a counter clockwise direction from the horizontal axis. The distance between the centers of the structuring element members at opposite ends of lines is taken to be '3'. Similarly, an angle of 0 degrees and length of '3' is assumed and calculations are made.

The input image is dilated using the two structuring elements at varying angles that returns the dilated image [14]. The domain of the composition of the two line structuring elements is determined by dilating the input image with both the structuring elements in sequence. Light structures connected to the image border are suppressed. The structures that are lighter than their surroundings and connected to the image border are suppressed. A default connectivity of '8' is assumed for 2-D images [14]. The operation reduces the overall intensity level in addition to suppressing the border structures. The image is morphologically opened to remove small objects. All connected components fewer than the specified number of pixels is removed, producing a noise-free output image. A value of '200' for the number of connected components removes noise from the image. A binary closure is performed where the image is dilated followed by an erosion operation. A 'flood-fill' operation is performed on the background pixels with the input binary image where the starting location is specified [15]. A hole is a set of background pixels that will not be reached by filling in the background from the edge of the image. The holes in the input image are filled by this operation. The algorithm is run with Matlab 7.12.0 in Pentium IV, 1.5 GHz Computer. The perimeter of the objects in the binary image is calculated and a binary image is obtained that contains only the perimeter pixels of objects in the input image. A non-zero pixel is part of the perimeter and is connected to a minimum of one zero-valued pixel. A default connectivity of '4' is assumed for the 2-D images. The resulting segmented image using the Boundary Mapping algorithm is shown in figure 2a and figure 2b. The algorithm returns a segmented image where each object in the image is uniquely identified and boundary mapped with accuracy.

3. Multidirectional Block Ranking

Using Boundary Mapping algorithm, the ROI is clearly identified. The image is subjected to the Multidirectional Block Ranking algorithm to remove the Interphase cells and other unwanted interferences. Considering an image of size n*n, various parameters for 'n' number of Horizontal (H) rows, 'n' number of Vertical (V) columns, and '2n-1' number of Positive (D2) and Negative Diagonals (D1) are evaluated. Figure 3a, Figure 3b and Figure 3c illustrates the computation of the parameters along the Horizontal and Vertical (H and V), Negative Diagonal (D1) and Positive Diagonal (D2) Directions respectively [16]. With such an evaluation, the contribution of individual blocks of an entire image, to the formation of the Region of Interest (RoI) is identified. Considering the presence of RoI in a particular image block, multiple parameters evaluated in different directions help assigning ranks to those blocks that contribute more to the formation of the RoI. Considering an image of size 4*4 (n=4), an object is found placed in (2, 2), (3, 2) and (3, 3). Parameters are evaluated in

horizontal, vertical and diagonal directions that helps identify the rows, columns and diagonals that contribute to the formation of the RoI. The presence is marked with 'P' and absence with 'A' for the corresponding rows, column and diagonal.

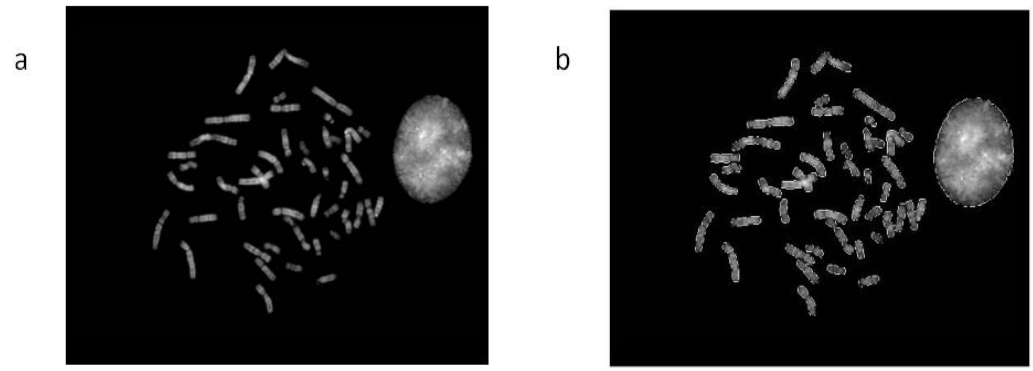

Figure 2. a) Image Containing Chromosomes and Interphase Cells; b) Boundary Mapping with the Proposed Mapping Algorithm

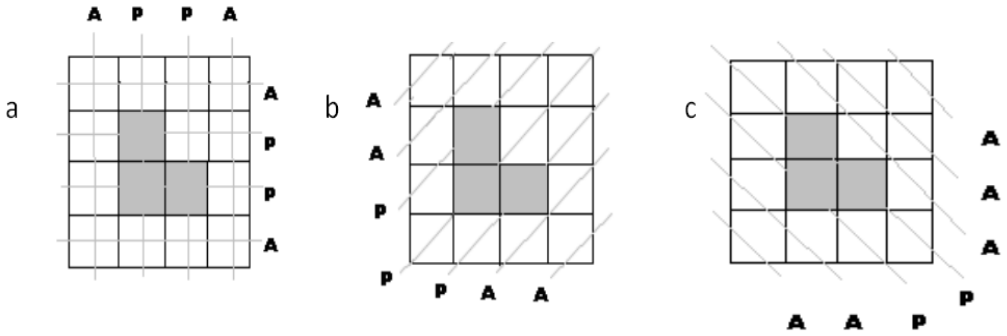

Figure 3. a) Evaluation in the Horizontal (H) and Vertical (V) Directions; b) Evaluation in the Negative Diagonal Direction (D1); c) Evaluation in the Positive Diagonal (D2) Direction

Multidirectional Block Ranking method assigns ranks to the blocks based on their contribution to the RoI. A rank is assigned to the blocks in the Horizontal (H), Vertical (V), Negative Diagonal (D1) and Positive Diagonal (D2) directions if the RoI is present. No rank is assigned for the absence of RoI. The Block Ranking table as shown in Table 1 shows a maximum rank of '4' is assigned to the blocks (2,2), (3,2) and 3,3), while the other blocks have lesser cumulative ranks. The cumulative ranks along the Horizontal (H), Vertical (V), Negative Diagonal (D1), Positive Diagonal (D2) and the sum values are tabulated. Blocks (2,2), (3,2) and 3,3) contribute to the RoI and thus a maximum rank of '4' is assigned to the blocks (2,2), (3,2) and 3,3) while the other blocks receive lesser ranks. The RoI is segmented by selecting those blocks whose ranks exceed a definite threshold. [17]

Table 1. Multidirectional Block Ranking

Block	Horizontal (H)	Vertical (V)	Negative Diagonal (D1)	Positive Diagonal (D2)	Sum
1,1				1	1
1,2		1			1
1,3		1	1		2
1,4			1		1
2,1	1			1	2
2,2	1	1	1	1	4
2,3	1	1	1		3
2,4	1		1		2
3,1	1		1		2
3,2	1	1	1	1	4
3,3	1	1	1	1	4
3,4	1				1
4,1			1		1
4,2		1	1		2
4,3		1		1	2
4,4				1	1

Supervised segmentation is performed wherein the range of values for the parameter of interest is evaluated for the segmented RoI. These parameters are used to evaluate the Gaussian Ranking Functions (GRF) that assigns a rank in the range [0, 10] based on the contribution of the block to the RoI. Figure 4 shows a typical Gaussian Ranking Function (GRF) with mean value ‘μ’ and standard deviation ‘σ’.

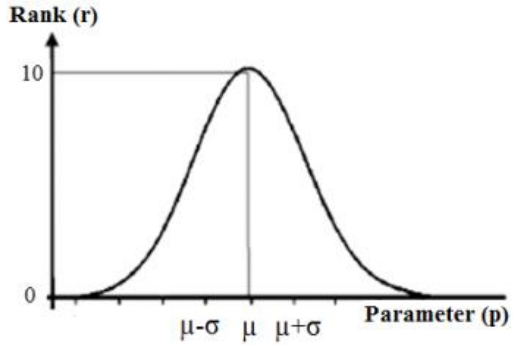

Figure 4. Gaussian Ranking Function (GRF) with mean value ‘μ’ and standard deviation ‘σ’

A block is assigned the maximum rank of ‘10’ when its characteristics exactly match that of the RoI. If we have ‘n’ parameters to be evaluated, there will be ‘n’ GRFs. ‘34’ parameters are evaluated in the Horizontal (H), Vertical (V), Negative Diagonal (D1) and Positive Diagonal (D2) directions that corresponds to generating ‘34’GRFs. A block is assigned a Gaussian Rank ‘r’ based on the relation:

$$r = abs[\left(\frac{1}{\sigma\sqrt{2\pi}} * \exp\left(-\frac{1}{2} * \left(\frac{p-\mu}{\sigma}\right)^2\right) * 10\right)]) \quad (1)$$

where ‘r’ is the Gaussian Rank, ‘p’ is the evaluated parameter, ‘μ’ is the Mean value of the parameter ‘p’ and ‘σ’ is the standard deviation. The Gaussian Rank is assigned to all the blocks that contribute to the parameter ‘p’. For each block, the parameters are evaluated in multiple directions and the GRFs are evaluated.

4. Feature Extraction

Structural feature parameters including the Mean (M), Standard Deviation (SD), Entropy (E), Skewness (S), Kurtosis (K), Second Central Moment (SCM), and Variance (V) are evaluated in diverse directions. Shape feature parameters including the Area (A), Perimeter (P), Eccentricity (E), Aspect Ratio (AR), Circularity (C), Elongation Shape factor (ESF), Compactness Shape Factor (CSF), Waiveness Shape Factor (WSF), and Isotropic Shape Factor (WASF) are evaluated in the Horizontal (H), Vertical (V), Negative Diagonal (D1) and Positive Diagonal (D2) directions [18-21]. An appropriate GRF is allotted to each block, based on their contribution to the formation of the RoI. Measuring these characteristic features for all the blocks in the given image helps in identifying and removing the Interphase cells exhibiting structural homogeneity with efficacy. The Entropy of a random variable ‘x’ is given by:

$$H(x) = -\sum \left[\!\left[P(x\_i\,]\!\right]\right) \left[\!\left[log\right]\!\right]\_b P(x\_i) \tag{2}$$

where P(x) is the probability associated with the random variable of interest and H(x) is the entropy of the random variable ‘x’. The Second Central Moment (SCM) of a real valued function g(x) of a real random variable about a value‘d’ is defined by:

$$\left[\!\left[\mu\right]\!\right]\_2\hat{}\sim = \int\_(-\infty)\hat{}\infty (x-d)\hat{}2 \; g(x)dx \tag{3}$$

Shape factors give the most accurate discrimination of the RoI. The most commonly used shape factors include the Area (A), Perimeter (P), Eccentricity (E), Aspect ratio (AR), Circularity (C), Elongation Shape Factor (ESF), Compactness Shape Factor (CSF), Waiveness Shape Factor (WSF), and Isotropic Shape Factor (WASF). Aspect Ratio is a normalized value that approaches zero for a stretched region of interest and close to one for a particle with equal axis. Elongation Shape Factor (ESF) is measured as the ratio of the second moments ‘J_n’ of the region of interest. The values of ‘AR’, ‘C’ and ‘ESF’ are mathematically given by:

$$AR = (Dia(\max))/(Dia(\min)) \tag{4}$$

$$C = (4 * \pi * \text{Area})/\text{Perimeter}\hat{}2 \tag{5}$$

$$ESF = \sqrt{(J\_2/J\_1)} \tag{6}$$

Compact Shape Factor (CSF) is measured as the ratio of the square of the area to the polar second moment ‘J_n’ of the RoI. A circular RoI has the maximum of one for the compactness shape factor.

$$CSF = A\hat{}2/(2 * \pi * \sqrt{(2\& \left[\!\left[J\_1\right]\!\right]\hat{}2 + \left[\!\left[J\_2\right]\!\right]\hat{}2)}) \tag{7}$$

Waiveness Shape Factor (WSF) is defined as the ratio of the convex portion of the perimeter of the region of interest to the total perimeter. It is mathematically defined as:

$$WSF = (\text{'P' Convex Portion})/(\text{Total 'P'}) \quad (8)$$

Isotropic shape factor (ISF) gives a measure of the regularity of the shape of the region of interest to its gravitational centre. The Isotropic shape factor for a 2-D shape with a maximum radius ' Max_R' and a minimum radius 'Min_R' is given by:

$$ISF = Min\_R/Max\_R \quad (9)$$

The cumulative rank (t) for each block from the GRFs is given by the sum of all ranks obtained by the blocks in a given image.

$$t = \sum\_(p = 1)^k r\_p \quad (10)$$

where 't' is the cumulative rank obtained by a block, 'p' is the parameter, 'r_p' is the rank for the 'p_{th}' parameter and 'k' is the total number of parameters. '32' parameters are evaluated in the Horizontal (H), and Vertical (V) directions and the two diagonal averages ($D1_{av}$ and $D2_{av}$) are measured in the Negative Diagonal (D1) and Positive Diagonal (D2) directions, contributing to a total of '34' parameters evaluated in all the directions. The maximum rank that a block will get is 10*34=340. A maximum rank of 340 is obtained by all those blocks that wholly contribute to the formation of RoI. A Rank Image 'R' is obtained by repeating the process of assigning ranks to all the blocks that contribute to the RoI. A binary image 'B' is obtained from the rank Image (R) by applying an appropriate rank threshold [17].

$$B(i,j) = 0; \quad R(i,j) >= \tau$$
$$1; \quad R(i,j) < \tau \text{ where '}\tau\text{' is the rank threshold}$$

The Segmented Image (S) is obtained by a point to point product of the Binary Image (B) with the Original Image (I).

$$S = B*I \quad (11)$$

Figure 5a, Figure 5b and Figure 5c shows an instance of segmentation of the object of interest based on the rank threshold.

5. Performance Evaluation

The effectiveness of the work is evaluated with the clinical database, made available by Grisan *et al.*, [22], at BIOIMLAB, University of Padova, Italy [23] and a comparative study with the other segmentation methods are performed. '172' intensity normalized chromosome images of dimensions 512*512 are selected for experimental study. The image is divided into blocks of size 8*8 and '34' parameters are evaluated, and the cumulative rank is calculated and assigned to all the blocks. Being a supervised algorithm, the system is initially trained with 50 samples, each being blocks of dimensions 89*89, containing the Interphase cells and debris that are structurally homogenous. The GRFs are evaluated from the Mean (μ) and Standard Deviation (σ) values for the '34' parameters for all the 50 samples. These values are taken as the central mean, standard deviation values for the calculation of the GRFs. Photomicrographs of dimensions 512*512 are divided into blocks of size 8*8, various other sizes of blocks are attempted for testing purposes, and the algorithm is applied to all the

blocks for rank calculation. The result of segmentation for a given image for the optimum block size 'n' of '4' and 'τ' of '324' is shown in the figure 6a and figure 6b.

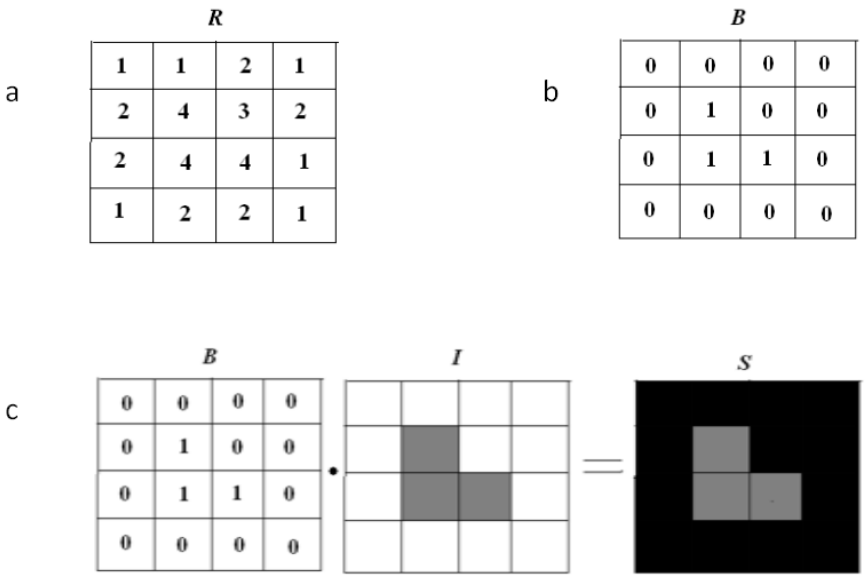

Figure 5. a) Rank Image (R); b) Binarized Rank Image (B); c) Segmentation of the RoI

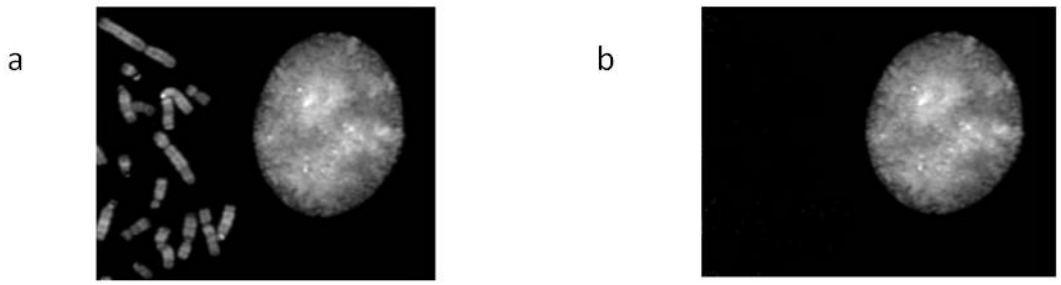

Figure 6. (a) Original Image (b) Optimum Segmentation with 'τ'=324 and 'n'=4

Figure 6b shows the segmentation of an Interphase cell with no chromosomes. The segmented Interphase is masked and the chromosomes are retained by applying a reverse threshold operation.

$$B(i,j) = 1; \quad R(i,j) >= \tau$$
$$0; \quad R(i,j) < \tau \text{ where '}\tau\text{' is the rank threshold}$$

The image obtained with this reverse threshold operation shows the chromosomes with no Interphase cells and any other kind of debris, facilitating segmentation and removal of unwanted interferences from the chromosome images. Figure 7 shows the result of a reverse operation where the chromosomes are present isolated from the Interphase cells, debris and other unwanted components, facilitating accurate, automatic segmentation.

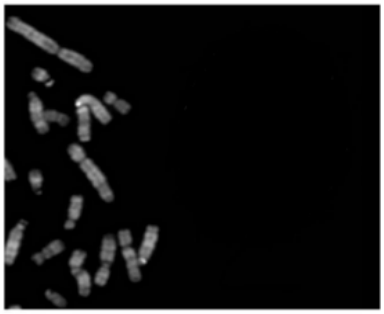

Figure 7. Chromosomes with No Interphase Cells and Debris

The accuracy of segmentation increases with the decrease in the size of the block for a given image. The algorithm accomplishes segmentation by making use of the contribution of individual blocks to the RoI based on the a-priori information about the parameters associated with the RoI and comparing this information with the evaluated parameters from the individual blocks. The size of the block and the threshold rank 'τ' is varied to modify the segmentation level. A total of '34' parameters are used with '10' being the maximum rank for an individual parameter, the maximum value for the threshold rank is '340'. Segmentation Accuracy (SA) is defined as the ratio of the area of the segmented RoI using the algorithm to the area of the manually segmented RoI.

$$SA = \frac{\text{Area of the segmented RoI using algorithm}}{\text{Area of manually segmented RoI}} \quad (12)$$

The variation in the rank threshold has its impact on the accuracy of segmentation. With decrease in threshold rank, spurious blocks are selected to contribute to the segmented mage. When the threshold rank is increased beyond a certain limit, the RoI to be segmented appears distorted. An optimum rank threshold of '324' is selected to accomplish the best Segmentation Accuracy (SA) of 98.4%. Figure 8a, Figure 8b, Figure 8c and Figure 8d show the variation in the Segmentation Accuracy (SA) with respect to the changes in the block size for an optimum rank threshold 'τ'=324.

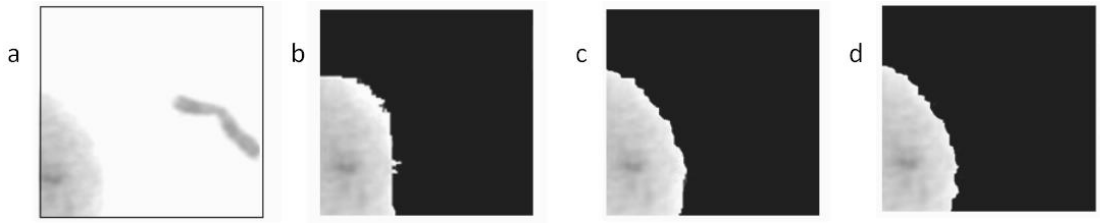

Figure 8. a) Original Image; b) Segmented Image for 'n'=16 and 'τ'=324; c) Segmented Image for 'n'=8 and 'τ'=324; (d) Segmented Image for 'n'=4 and 'τ'=324

The variation in rank threshold plays a crucial role in deciding the Segmentation Accuracy. Figure 9a and 9b show distorted results owing to over and under segmentation respectively and Figure 9c shows optimum segmentation for a value of 'n'=4 and 'τ'=324.

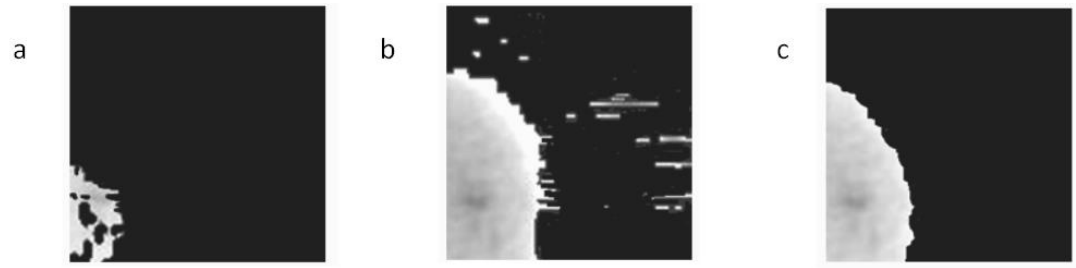

Figure 9. (a) Over Segmentation for 'n'=4 and 'τ'=340 (b) Under Segmentation for 'n'=4 and 'τ'=260 (c) Optimum Segmentation for 'n'=4 and 'τ'=324)

The effect of variations in rank threshold for a given block size of 'n'='4' is shown in Table 2 and Table 3 gives an analysis of time taken for segmentation using the algorithm for an optimum rank threshold of 'τ'=324. The size of the input image is 512*512 and the algorithm is run on Matlab 7.12.0 in Pentium IV, 1.5 GHz Computer. Table 2 and Table 3 clearly depicts the changes or the effect of variations in the rank threshold for a given block size and the analysis of time for an optimum rank threshold. An optimum threshold value of '324' is chosen to prevent distortions in the output image.

Table 2. Effect of Variations in Rank Threshold for a Given Block Size of n=4

Threshold Rank	Segmentation Accuracy (SA) in %	Segmentation Type
340	74.3	Over
324	98.4	Optimum
300	90.2	Under
285	78.7	Under
260	74.6	Under

Table 3. Time Analysis for an optimum rank threshold of τ=324

Block Size (n)	Segmentation Accuracy (SA) in %	Time taken for Segmentation (in sec)
64	90.2	13
32	91.8	21
16	94.3	26
8	96.7	33
4	98.4	48

6. Results and Discussions

In cases where conventional thresholding techniques fail to perform accurate segmentation, the Multidirectional Block Ranking algorithm is employed to segment the RoI, from the given image. Segmentation techniques like region growing, active contours, snakes and deformable models require initial placement of seeds and contours respectively, around the RoI, but the Multidirectional Block Ranking algorithm will not necessitate prior locating of the RoI. The Interphase cells are uniquely identified and removed, facilitating error-free karyotyping procedures. Figure 10 shows the segmentation accuracy achieved with the traditional segmentation techniques.

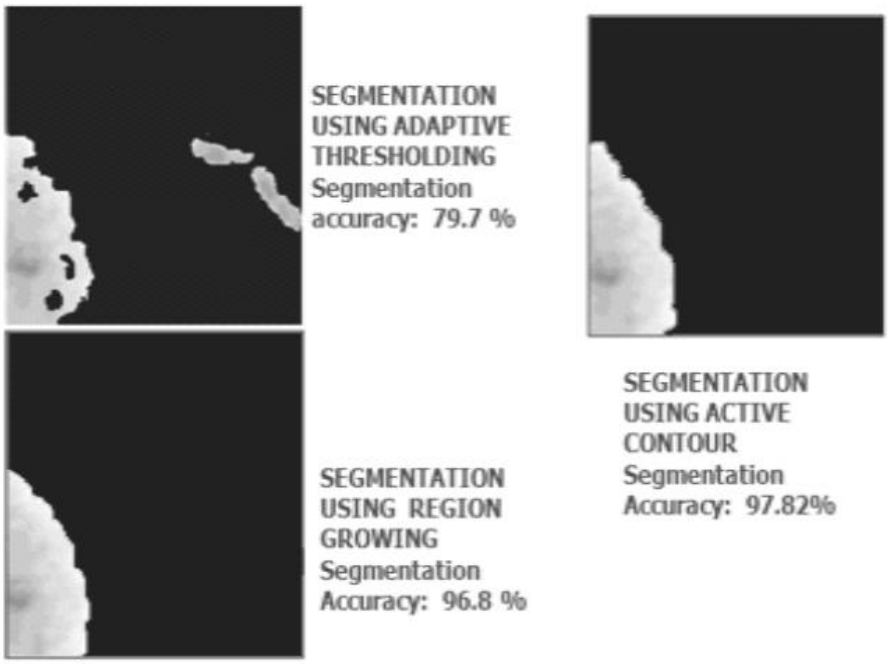

Figure 10. Results showing usage of conventional segmentation methods

The results of comparison with other conventional methods of segmentation is shown in Table 4 and a time comparison of the various segmentation methods is shown in Table 5. The Multidirectional Block Ranking algorithm is highly efficient in segmenting structurally homogenous objects in comparison to other segmentation techniques. The size of the image is 512*512 and the algorithm is run on Matlab 7.12.0 in Pentium IV, 1.5 GHz Computer.

Table 4. Comparison with Other Methods of Segmentation

Method	Segmentation Accuracy in %	Remarks
Active Contours	97.82	Initial placement of contour around the RoI
Region Growing	96.8	Initial placement of seed around the RoI
Adaptive Thresholding	79.7	Inability to differentiate between portions of interphase cells and chromosomes
Segmentation using Multidirectional Block Ranking	98.4	Prior location of RoI not required and Interphase cells are uniquely identified and removed

Table 5. Time Comparison

Method	Time taken to produce segmented output (s)	Remarks
Active Contours	16	Excluding the time taken for initial placement of seed and contour
Region Growing	12	
Adaptive Thresholding	19	Equal Block Size
Multidirectional Block Ranking	48	

7. Future Enhancements

Inclusion of additional statistical and structural parameters will be considered for the future work with M-FISH and CGH chromosome images that can further increase the Segmentation Accuracy of the algorithm and aid cytogenetic experts in diagnosing genetic disorders with the best accuracy.

Acknowledgements

We extend our sincere thanks to Grisan *et al.*, [22] for helping us with the standardized database of pro-metaphase chromosomes for the successful completion of the work.

References

[1] S. Rajaraman and A. Chokkalingam, International Journal of Bioscience and Biotechnology, vol. 1, no. 1, **(2013)**.
[2] J. Piper and E. Graham, Cytometry Mag., vol. 10, no. 3, **(1989)**.
[3] S. W. Katz and A. D. Brink, Editors, "Segmentation of chromosome Images", IEEE South African Symposium on Communications and Signal Processing, Johannesburg, South Africa, **(1993)** August 6.
[4] ISCN: An international system for human cytogenetic nomenclature. Cytogenet. Cell Genetics, **(1985)**.
[5] M. Thompson, R. McInnes and H. Willard, Genetics in Medicine, Saunders, Kingston **(2005)**.
[6] B. Lerner, IEEE Trans. Syst. Man Cybern., vol. 28, **(1998)**.
[7] J. Liang, Cytometry, vol. 17, **(1994)**.
[8] P. Mousavi, R. K. Ward, S. S. Fels and M. Sameti, IEEE Trans. Biomedical Engineering, vol. 49, no. 4, **(2002)**.
[9] M. P. Sampat, A. C. Bovik, J. K. Aggarwal, K. R. Castleman, Pattern Recog., vol. 38, **(2005)**.
[10] Q. Wu, "Automated Identification of Human Chromosomes as an Exercise in Building Intelligent Image Recognition Systems", Doctoral Dissertation, Catholic University of Leuven, Belgium, **(1987)**.
[11] A. P. Reeves, R. J. Prokop, S. E. Andrews and F. P. Kuhl, IEEE Trans. Pattern Analysis and Machine Intelligence, vol. 10, **(1988)**.
[12] N. Otsu, IEEE Trans. Syst., Man, Cybern., vol. 9,no. 1, **(1979)**.
[13] T. Jorgensen, IEEE Trans. Aerospace and Electronic Systems, vol. 46, no. 4, **(2010)**.
[14] A. K. Jain, Editor, "Fundamentals of Digital Image Processing", Prentice Hall, New Jersey, **(1998)**.
[15] Nosal and Eva-Marie, Editors, "Flood-fill algorithms used for passive acoustic detection and tracking", New Trends for Environmental Monitoring Using Passive Systems, Univ. of Hawaii, Honolulu, HI, **(2008)** October 14-17.
[16] P. Felzenszwalb and D. Huttenlocher, Editors, "Image segmentation using local variation", Proceedings of IEEE Conference on Computer Vision and Pattern Recognition, Santa Barbara, CA, USA, **(1998)** June 25.
[17] R. C. Gonzalez, R. E.Woods and S. L. Eddins, "Digital Image Processing using Matlab", Edited R. C. Gonzalez, Prentice Hall Publishers, New Jersey, **(2003)**, pp. 92-95.
[18] I. Jermyn and H. Washikawa, IEEE Trans. Pattern Analysis and Machine Intelligence, vol. 23, **(2001)**.

[19] J. M. Morel and S. Solimini, "Bulletin (New Series) of the American Mathematical Society", vol. 33, no. 2, **(1996)**.
[20] W. Schwartzkopf, B. L. Evans and A. C. Bovik, Editors. "Entropy Estimation for Segmentation of Multi-Spectral Chromosome Images", Fifth IEEE Southwest Symposium on Image Analysis and Interpretation, Washington DC, USA, **(2002)** April 7-9.
[21] W. Schwartzkopf, A. C. Bovik, and B. L. Evans, IEEE Trans. Med. Imag., vol. 24, no. 12, **(2005)**.
[22] E. Grisan, E. Poletti and A. Ruggeri, IEEE Trans. Inf. Technol. Biomed., vol. 13, no. 4, **(2009)**.
[23] Laboratory of Biomedical Imaging, University of Padova, Italy, available at http://bioimlab.dei.unipd.it: Accessed April, **(2012)**.

Authors

Sivaramakrishnan Rajaraman graduated in the discipline of Electronics and Communication Engineering from Madurai Kamaraj University and completed his Post Graduation in Medical Electronics from Anna University, Chennai, India. He has more than 11 years of teaching experience to his credit in diverse areas of electronics, communication, biomedical and medical electronics. His work on "Early Detection of Cancer using Fuzzy Based Photoplethysmography" has received the prestigious AT&T BELL LABORATORIES AWARD from USA, with a cash grant. He has published various papers at graduate and post graduate levels in national and international journals and conferences. His research areas include image processing, EEG Signal Analysis, and Brain Computer Interface analysis.

Ganesh Vaidyanathan is currently heading the department of electronics and communication engineering at Sri Venkateshwara College of Engineering, Sriperumbudur. He completed his under graduation at Sri Venkateshwara College of Engineering, Sriperumbudur and pursued his Masters in Electronics and Control at Birla Institute of Technology and Science, Pilani. He completed his PhD at Anna University, Chennai and submitted a thesis on Evolution and performance evaluation of processing techniques for automatic Karyotyping. He has more than 20 years of experience in the teaching field and his areas of interest are Mechatronics, Pattern Recognition and Artificial Intelligence.

Arun Chokkalingam received his B.E. Degree in Electronics and Communication Engineering from Shanmuga College of Engineering, India and completed his Post Graduation in Applied Electronics at PSNA College of Engineering and Technology, Dindigul, India. He has completed his Ph.D. under the Information and Communication Discipline in 2010. He has published various papers at graduate, post graduate and doctorate levels in national and international journals and conferences. His research areas include VLSI Signal Processing, Image Processing, and Digital Communication.